HYDROLOGICAL PROCESSES
Hydrol. Process. **29**, 1027–1045 (2015)
Published online 18 May 2014 in Wiley Online Library
(wileyonlinelibrary.com) DOI: 10.1002/hyp.10217

Conditioning temperature-index model parameters on synoptic weather types for glacier melt simulations

T. Matthews,[1]* R. Hodgkins,[2] R. L. Wilby,[2] S. Guðmundsson,[3] F. Pálsson,[3] H. Björnsson[3] and S. Carr[4]

[1] *Department of Geography, National University of Ireland, Maynooth, Kildare, Ireland*
[2] *Department of Geography, Loughborough University, Loughborough, UK*
[3] *Institute of Earth Science, University of Iceland, Reykjavík, Iceland*
[4] *School of Geography, Queen Mary University of London, London, UK*

Abstract:

Temperature-index models are widely favoured as a pragmatic means of simulating glacier melt because of their generally good performance, computational simplicity and limited demands for *in situ* data. However, their coefficients are normally treated as temporally stationary, unrealistically assuming a constancy of the prevailing weather. We address this simplification by prescribing model coefficients as a function of synoptic weather type, in a procedure that utilizes reanalysis data and preserves the minimal data requirements of temperature-index models. Using a cross-validation procedure at Vestari Hagafellsjökull, Iceland, and Storglaciären, Sweden, we demonstrate that applying transient model coefficients, for three temperature-index models, results in statistically significant increases in the skill with which melt is modelled: Median simulation improvements in the Nash–Sutcliffe efficiency coefficient of 7.3 and 23.6% are achieved when hourly and daily melt totals are evaluated respectively. Our weather-type modelling approach also yields insight to processes driving parameter variability, revealing dependence that is consistent with a priori considerations of the surface energy balance. We conclude that incorporating weather types into temperature-index models holds promise for improving their performance, as well as enhancing understanding variability in coefficient values. Copyright © 2014 John Wiley & Sons, Ltd.

KEY WORDS temperature index; glacier melt modelling; weather types; glacier–climate interactions; nearest-neighbour resampling

Received 25 July 2013; Accepted 10 April 2014

INTRODUCTION AND AIMS

Melting snow and ice have far reaching and important societal consequences, not least for water and energy security of communities. Physically, the consumption of latent heat, decline in surface albedo and impact on the hydrological cycle caused by this phase change have implications for the Earth–atmosphere system as a whole. Quantifying glacier melt rates has, therefore, received much attention, with particular focus on modelling studies.

Generally, models calculate the melt rate either from principles of energy conservation (*energy balance models*) or from empirical associations between meteorological variables and surface melting. Most commonly, empirical formulations exploit the correlation between melt and air temperature (*temperature-index models*). Whilst a physical approach to melt modelling is conceptually desirable, it is often impractical to apply in practice because of the detailed knowledge of the local micrometeorology and snow/ice surface properties demanded.

Empirical, temperature-based melt models have less stringent data requirements. Measurements of air temperature are widely available, and this variable is also relatively straightforward to interpolate and forecast (Hock, 2003). Despite their simplicity, temperature-index approaches also generally perform well in melt simulations – often matching or exceeding the skill of energy balance models (Hock, 2005; Zhang *et al*., 2012). Thus, temperature-index models are applied widely in cryospheric research and notably in assessing likely future melt rates for the world's glaciers (Raper and Braithwaite, 2006; Radić and Hock, 2011; Dobler *et al*., 2012; Marzeion *et al*., 2012). Because rising air temperature is one of the most likely consequences of anthropogenic climate change (Meehl *et al*., 2007; Maraun *et al*., 2010), these models are conceptually well placed for such application.

At their most basic, temperature-index models take the general form (e.g. Hodgkins *et al*., 2012):

*Correspondence to: Tom Matthews, Department of Geography, National University of Ireland, Maynooth, Kildare, Ireland.
E-mail: tom.matthews@nuim.ie

$$M = \begin{cases} MF_{snow/ice}\mathrm{T} & : \mathrm{T} > T_c \\ 0 & : \mathrm{T} \leq T_c \end{cases} \quad (1)$$

where T is air temperature (°C), and T_c is a threshold air temperature, above which melting occurs at a rate governed by the melt factor (*MF*). The subscripts indicate that different values are applicable, depending on whether the melting surface is snow or ice. Time periods of a day are frequently used for the relation described by Equation (1): T is then averaged to daily resolution, and the *MF* has units of mm water equivalent (w.e.) $°C^{-1}$ day^{-1}. If a threshold of 0 °C is defined, the *MF* is usually termed the 'degree-day factor' (*DDF*), and air temperatures over T_c are known as 'positive degree days' (PDDs: Hock, 2003).

More elaborate empirical formulations are provided by enhanced temperature-index models (ETIs) (Cazorzi and Fontana, 1996; Hock, 1999; Daly *et al*., 2000; Pellicciotti *et al*., 2005), which typically include a term to reflect changes in the shortwave radiation balance – the dominant source of melt energy for most alpine glaciers (Willis *et al*., 2002). ETI models often outperform traditional approaches (e.g. Equation (1)) in intercomparison studies by better accounting for spatial and temporal variability in melt rates (Cazorzi and Fontana, 1996; Hock, 1999; Pellicciotti *et al*., 2005).

Whilst the provision for changes in the shortwave heat flux in ETI models offers both a conceptual and practical improvement to temperature-index melt simulations, they retain some important limitations. ETIs and their more basic counterparts usually employ temporally static coefficients. With regard to the *DDF*, this treatment has long been recognized as physically unrealistic (Lang and Braun, 1990, Braithwaite, 1995; Hock, 2003), as its value depends on the surface energy balance (SEB) and hence on the prevailing weather. Carenzo *et al*. (2009) confirmed that the same is true of parameters in the Pellicciotti *et al*. (2005) ETI model. More recently, Carturan *et al*. (2012) and Irvine-Fynn *et al*. (2014) also highlighted the role of variable weather types as possibly responsible for the limited interannual transferability of calibrated ETI model parameters.

To reduce the detrimental effect of parameter sensitivity to weather types, Lang and Braun (1990) recommended extensive periods of integration to calibrate *DDFs* to obtain values more appropriate for sites' 'average weather'. This same reasoning can be extended to the calibration of parameters within ETI models. However, as interannual synoptic variability can be high in mid-latitudes and high latitudes (Fettweis *et al*. 2011), in practice, it may be challenging to identify calibration periods representative of long-term average conditions. Moreover, in the context of climate change, 'average weather' is not expected to be stationary, making this calibration philosophy questionable for simulations of future glacier melt.

A more conceptually appealing approach to temperature-index melt modelling would be to account for the effect of different weather types on parameters explicitly, by prescribing transient values appropriate to the prevailing weather. However, provisioning for the effect of weather types on model parameters implies a need for additional knowledge of local micrometeorology. Such information is not necessarily available in remote locations typical of glacierized regions. Thus, practical steps to integrate the effect of weather types on temperature-index model parameters should seek to preserve their low demands for *in situ* data.

In this study, we show how the effect of weather types on temperature-index model parameters can be incorporated without the need for additional meteorological measurements from the glacier boundary layer. To achieve this, temperature-index models are conditioned on synoptic weather types derived from gridded climate data. The skill of weather-type-dependent models is assessed relative to unmodified temperature-index models. Variation in model parameters between weather types is also evaluated to gain insight to meteorological controls on their temporal evolution.

DATA AND METHODS

Conditioning temperature-index model parameters by weather type requires high-resolution information on glacier melt rates and the prevailing meteorology. Details of these datasets are provided in this section, along with a description of the procedure for defining weather types and the process for evaluating the utility of transient model parameters.

Glacier melt rates

Our data are obtained from Vestari Hagafellsjökull, Iceland, and Storglaciären, Sweden. Melt rates from both glaciers are determined from SEB simulations conducted with a physically based model. We use these data rather than melt estimates from measurements at ablation stakes or acoustic sounders because the latter can be prone to substantial error when converting to water equivalent at high temporal resolution (Müller and Keeler, 1969; Munro, 1990; Arendt and Sharp, 1999; Pellicciotti *et al*., 2005).

The meteorological measurements and SEB calculations are described in detail by Matthews (2013) and are summarised here. Ablation-season meteorological observations on Vestari Hagafellsjökull (Langjökull) have been logged hourly by automatic weather stations (AWSs) installed by the Institute of Earth Sciences, University of Iceland, in 2001. One station is located in the lower ablation zone at ~500 m.a.s.l (VH 500) and the other at 1100 m.a.s.l (VH 1100), the approximate elevation of Langjökull's average equilibrium line altitude. Here, we use data from

June–August for the years 2001–2007 at VH 500 and from 2001–2009 at VH 1100. Sensor specifications are provided in Table I, and further details of the measurement campaign can be found in Guðmundsson *et al.* (2009).

At Storglaciären, detailed AWS observations were made in the upper ablation area (~1387 m.a.s.l) on the glacier during July–August 2011 (Figure 1), and more limited data acquisition took place in 2010 (Table I). Interannual

Table I. Details of the sensors deployed at the glacier automatic weather stations

Measurement (height)	Sensor	Accuracy (±)	Period that data used relates to (Julian day, year)
	Vestari Hagafellsjökull		
Air temperature (2 m)	Vaisala HMP35	0.2 °C	VH 500: 152–243, 2001–2007
Relative humidity (2 m)	Vaisala HMP35	2%	
Wind speed (2 m)	R.M. Young 05103	0.3 m s^{-1}	
Shortwave radiation (2 m)	Kipp and Zonen CNR1, CM3	3%	VH 100: 152–243; 2001–2009
Longwave radiation (2 m)	Kipp and Zonen CNR1, CG3	3%	
Ablation (variable)	Cambell Scientific SR50	Max(0.01 m, 0.4%)	VH 500: 152–243, 2001–2005; 191–243, 2006; 152–243, 2007 VH 1100: 152–243, 2001–2007; 152–235, 2008; 152–243, 2009
	Storglaciären		
Air temperature (2 m)	Vaisala HMP45C	0.3 °C at 0 °C	192–243, 2010; 191–243, 2011
Relative humidity (2 m)	Vaisala HMP45C	2% (0–90%); 3% (90–100%)	192–243, 2010; 191–243, 2011
Wind speed/direction (2 m)	Young 05103	0.3 m s^{-1}	192–243, 2010; 191–243, 2011
Shortwave radiation (1.5 m)	Kipp and Zonen CM7B	8%	192–243, 2010
	Kipp and Zonen CNR1, CM3	3%	191–243, 2011
Longwave radiation (1.5 m)	Kipp and Zonen CNR1, CG3	3%	191–243, 2011
Ablation (variable/*NA*)	Campbell Scientific SR50	Max(0.01 m, 0.4%)	196–243, 2011
	Manual stake measurements	Estimated: 5 mm	192–243, 2010; 191–243, 2011

Locations are indicated in Figure 1.

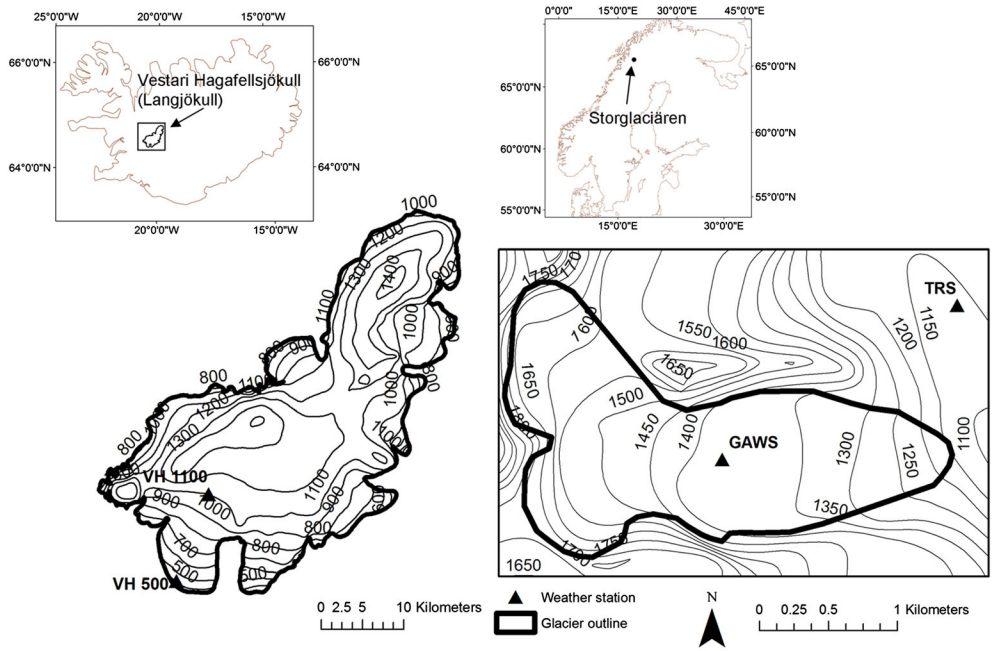

Figure 1. Location of study sites. Vestari Hagafellsjökull is an outlet of the Langjökull Ice Cap: The outline of the entire ice cap is shown on the left-hand side of the figure. Note that both the glacier AWS on Storglaciären (GAWS) and the AWS at the Tarfala Research Station (TRS) are shown on the right-hand side of the figure. Only the scale varies between the left and right sides of the figure (shown by the separate scale bars); both maps share the same legend

variability in the SEB can be pronounced at Storglaciären, as a result of differing meteorological conditions (Hock and Holmgren, 2005). Thus, we consider it valuable to extend this two-season record, to sample a wider variety of weather types. Extending our record of glacier meteorology is made possible because of the AWS at the proximate Tarfala Research Station (TRS: Figure 1).

Because TRS is situated outside the glacier boundary, judicious adjustment of the data measured there is required to infer glacier meteorology. To this end, the empirical functions applied by Matthews (2013) are used to adjust hourly mean values of air temperature, vapour pressure, wind speed and the incident shortwave flux recorded at TRS, to the location of the glacier-based AWS. The incident longwave flux is not measured at TRS, so it is determined for the glacier site following the expressions of Sedlar and Hock (2009). Albedo is assumed invariant outside the period of glacier-based observations and is prescribed as the mean ice albedo obtained from measurements (0.38). This treatment neglects any changes in surface reflectivity or roughness that may result from snowfall.

Parameterized meteorological series are used to infer glacier meteorology for periods when direct observations are unavailable in July and August, 2005–2011 (Table II). 2005 is chosen as the earliest year from which to use TRS data because of heterogeneity in the shortwave radiation record prior to this date (Matthews, 2013). Further information regarding the meteorological measurement campaign at TRS can be found in Grudd and Schneider (1996) and Jonsell *et al*. (2013).

A summary of agreement between the meteorology observed on-glacier and that parameterized from the TRS data is shown in Table III using the Nash–Sutcliffe efficiency coefficient (R^2: refer to Section on Temperature-Index Models). With the exception of hourly means of wind speed and incident longwave radiation, correspondence between series is encouraging. However, because of the imperfect fit, use of these data in our energy balance simulation introduces error to our reference melt series that will propagate to our temperature-index melt simulations (discussed in Section on Study Limitations and Transferability of the Modelling Approach).

Table III. Agreement between the parameterized meteorological variables for the location of the glacier AWS on Storglaciären (determined through empirical adjustment of observations made at TRS) and the meteorology measured on the glacier

	R^2(hourly)	R^2(daily)
Air temperature	0.873	0.946
Vapour Pressure	0.855	0.938
Wind Speed	0.416	0.670
Shortwave radiation	0.746	0.881
Longwave radiation	0.493	0.794

Agreement is presented in terms of the Nash–Sutcliffe efficiency coefficient (Equation (4)). R^2 is calculated for hourly and daily means (left-hand and right-hand columns respectively), for the period when glacier observations are available (Table II).

Details of SEB computations for both sites are provided in Table IV. Models are validated by comparing simulated cumulative water equivalent ablation with totals estimated from observations of surface lowering, converted to water equivalent through the empirical formulation outlined in Hodgkins *et al.* (2012). Using plausible values of the surface roughness length for momentum, taken from previous investigations at our study sites (Hock and Holmgren, 1996; Guðmundsson *et al*., 2009), our energy balance models are able to simulate melt totals, which, within estimates of their uncertainty, agree with observations (Figure 2). No tuning of model parameters (e.g. roughness lengths) was therefore considered necessary.

No direct observations of surface lowering are available at our study site on Storglaciären prior to 2011 (when the SEB model is forced with the parameterized meteorological series from TRS); hence, validation of model performance is not possible for this period. To investigate the effect of using this series, rather than the observations made at the glacier AWS, we can compare SEB model results when simulations are forced by both series for the period when glacier observations are available (Figure 3). The good overall correspondence between melt simulated with these series

Table II. Details of the data series used to force the SEB model on Storglaciären for different time periods

Data used for SEB simulation	Period (hour, Julian day, year)
Adjusted TRS meteorological series (all variables)	01:00, 182, 2005–14:00, 192, 2010; 01:00, 182, 2011–13:00, 191, 2011
Incident longwave radiation parameterized using the expressions of Sedlar and Hock (2009); all other meteorological variables taken directly from observations at glacier AWS	15:00, 192, 2010–24:00, 243, 2010
Observations at glacier AWS (all variables)	14:00, 191, 2011–24:00, 243, 2011

The 'adjusted TRS' meteorological series relates to those variables that are observed at the Tarfala Research Station and adjusted to the location of the glacier AWS using empirical functions. Refer to the text in Section on Glacier Melt Rates for further information.

Table IV. Details of the SEB computations used to determine the reference melt series at each location

Model for calculating the SEB (Q) at hourly time step: $Q = Q_H + Q_L + Q_{SW} + Q_{LW}$				
SEB component	Procedure for calculation	Associated parameters	Treatment at Vestari Hagafellsjökull	Treatment at Storglaciären
Turbulent heat flux (sensible: Q_H and latent: Q_L)	Bulk aerodynamic method	Roughness length of momentum	Ice: 10 mm Firn: 2 mm Snow: 0.1 mm	Ice: 2.7 mm Snow: 0.15 mm
		Roughness lengths of water vapour and temperature	Modelled according to Andreas (1987).	Modelled according to Andreas (1987)
		Stability corrections for turbulent heat flux calculations	Non-linear expressions of Beljaars and Holtslag (1991) used for stable conditions (glacier surface temperature below air temperature); equations of Paulson (1970) and Dyer (1974) applied for unstable case.	Neutral stratification assumed
		Glacier surface temperature	Assumed to be at the melting point (0 °C).	Assumed to be at the melting point when the longwave radiation balance is measured at the glacier AWS; zero-degree assumption also assumed when parameterized TRS data used to drive the SEB models, unless negative Q is encountered: In this case, the surface temperature is lowered iteratively (−0.25 °C steps) until $Q = 0$
Net shortwave heat flux (Q_{SW})	Incident flux minus reflected flux	Albedo	*NA* (radiation balance measured directly at AWS)	Direct observations used when available. Otherwise (when the parameterized TRS data are used to force the SEB model), albedo is prescribed as the mean ice albedo observed during the period of glacier AWS operation
Net longwave heat flux (Q_{LW})	Incident flux minus the flux emitted by the glacier surface	Emitted longwave radiation	*NA* (radiation balance measured directly at AWS)	Direct observations used when available. Otherwise (when the parameterized TRS data are used to force the SEB model), calculated from the glacier surface temperature using the Stefan Boltzmann law and assuming unit emissivity

Further information regarding the choice of model structure and parameter values can be found in Matthews (2013) and in Section on Glacier Melt Rates.

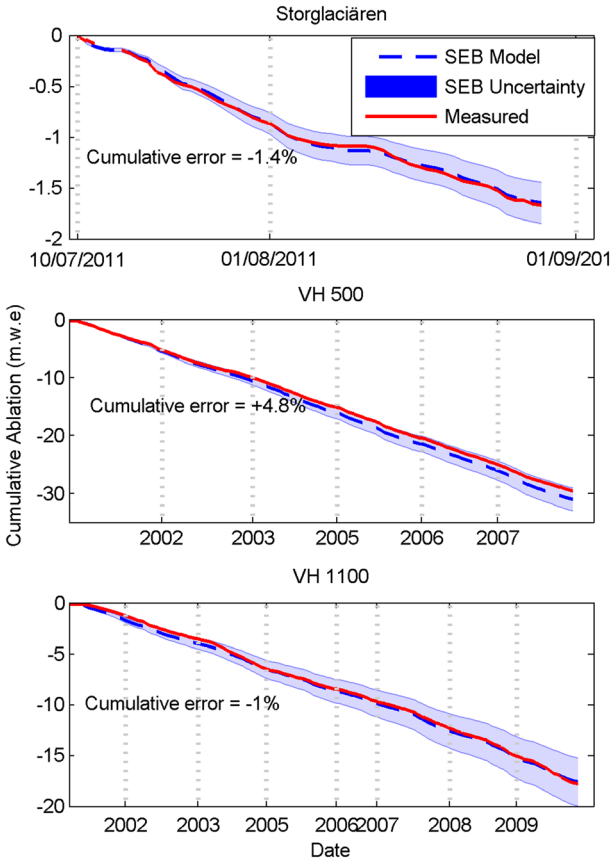

Figure 2. Comparisons of cumulative ablation simulated by the SEB models and estimated from measurements of surface lowering converted to water equivalent (Section on Glacier Melt Rates). Uncertainty in simulated ablation is estimated from the sensor uncertainties following the method outlined in Greuell and Smeets (2001). Note that periods when accumulation was observed are removed from the comparison at Vestari Hagafellsjökull, which accounts for the uneven length of annual series at VH 1100

provides confidence in the utility of using the parameterized TRS data to extend our reference melt series. With the addition of the melt rates calculated from adjusted TRS data, the reference melt series constitutes 434 days at Storglaciären; the records from VH 500 and VH 1100 comprise 644 and 828 days respectively. All these lengths are denoted *N* hereafter. Summaries of the meteorology and calculated energy components for the respective locations over these periods are provided in Table V.

Reanalysis data

We use gridded reanalysis data (ERA-Interim: Dee *et al.*, 2011) to determine synoptic weather types. The variables chosen to categorize daily weather are 2-m air temperature (°C), 2-m dewpoint air temperature (°C), 10-m U component of wind speed ($m\,s^{-1}$), 10-m V component of wind speed ($m\,s^{-1}$), total cloud cover (fraction) and sea level air pressure (Pa). These include most of those variables chosen frequently to characterize the prevailing meteorology in weather-type/air-mass identifications (e.g. Kalkstein and Corrigan, 1986; Sheridan, 2002; Bower *et al.*, 2007; Fealy and Sweeney, 2007). The reanalysis data were obtained at six-hourly resolution from grid cells overlying the field sites.

The selected variables were transformed to *z*-scores and subject to a principal component (PC) analysis. Five PCs were retained accounting for >80% of the variance in the original variables. The six-hourly reanalysis meteorology and PC loadings were then used to determine daily PC scores following Kalkstein and Corrigan (1986). These PC scores are used to identify periods of comparable weather in the algorithm described below (Section on Temporally Variable Model Coefficients).

Temperature-index models

Three temperature-index models are deployed to investigate the utility of using melt parameters conditioned by synoptic weather types. The first is the basic melt formulation outlined in Equation (1), referred to as Model 'A' hereafter. The others are ETI models, namely the algorithms of Hock (1999; hereafter model 'B'), and Pellicciotti *et al.* (2005; hereafter model 'C'). Our choice of models includes those

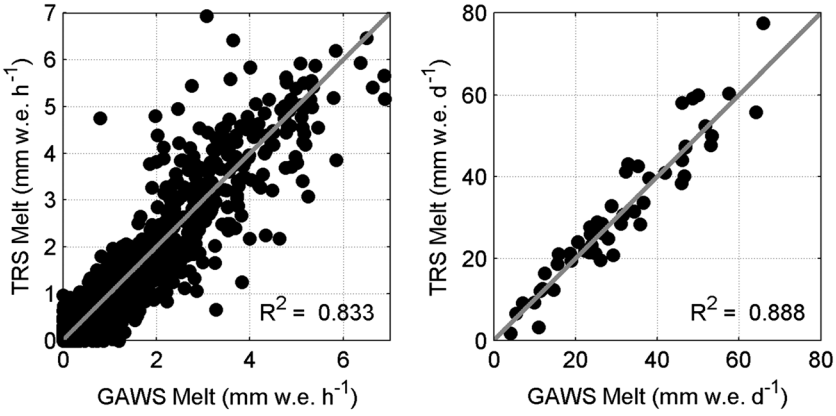

Figure 3. Comparisons of melt simulated by the SEB model at Storglaciären when forced with meteorological variables recorded on-glacier and when forced with the adjusted TRS meteorological series (GAWS and TRS melt respectively). R^2 is defined in Equation (4)

Table V. Mean meteorology and SEB components for the locations of the glacier AWSs (± standard deviation)

	VH 1100 (±σ)	VH 500 (±σ)	Storglaciären (±σ)
Period	June–August, 2001–2009	June–August, 2001–2007	July–August, 2005–2011
Air temperature (°C)	2.0 (1.4)	5.3 (1.3)	5.1 (2.5)
Wind speed ($m\,s^{-1}$)	5.4 (2.8)	5.3 (1.8)	2.9 (1.3)
Mixing ratio ($g\,kg^{-1}$)	4.7 (0.5)	5.0 (0.6)	4.6 (1.7)
Incident shortwave radiation ($W\,m^{-2}$)	200 (86.3)	163 (92.9)	158 (81.8)
Reflected shortwave radiation ($W\,m^{-2}$)	104 (61.0)	12.6 (24.3)	62.1 (32.8)
Albedo (dimensionless)	0.60 (0.13)	0.10 (0.10)	0.40 (0.10)
[a]Cloud cover (fraction)	0.48 (0.18)	0.58 (0.21)	0.60 (0.19)
Incident longwave radiation ($W\,m^{-2}$)	311 (30.9)	316 (28.0)	302 (24.5)
Emitted longwave Radiation ($W\,m^{-2}$)	311 (4.8)	315 (1.5)	314 (4.2)
[b]Emissivity (fraction)	0.81 (0.09)	0.92 (0.08)	0.89 (0.07)
Sensible heat flux ($W\,m^{-2}$)	20.2 (21.9)	70.0 (29.5)	38.6 (19.0)
Latent heat flux ($W\,m^{-2}$)	6.6 (16.4)	28.1 (22.2)	13.3 (16.6)
[c]RMSE (mm w.e. day^{-1})	10.8	13.9	11.4
[d]Melt (mm w.e. day^{-1})	29.8 (12.7)	65.1 (19.8)	34.9 (14.9)

Note that for Storglaciären, these results reflect meteorological data recorded *in situ* and TRS data adjusted to the glacier location (refer to Table II for the associated time periods).
[a] Cloud cover is defined as the mean ratio of received to potential, clear-sky global radiation.
[b] Thermal emissivity is defined as the mean ratio of received incident longwave radiation to that emitted by a blackbody radiator at the 2-m air temperature.
[c] The RMSE refers to the error in simulated ablation and
[d] gives the mean melt according to the SEB models.

used most frequently for purposes of glacier melt modelling, while differences in structure and data requirements facilitate insight into how our weather-type approach may contribute to more robust and accurate temperature-index melt simulations.

Model B has the form

$$M = TMF \cdot \mathrm{T} + RTMF \cdot \mathrm{I_{o/p}}(1-\alpha)\mathrm{T} \qquad (2)$$

and model C is

$$M = TMF \cdot \mathrm{T} + RMF \cdot \mathrm{I_{o/p}}(1-\alpha) \qquad (3)$$

where M is melt ($mm\,w.e.\,hr^{-1}$), TMF is the temperature melt factor ($mm\,w.e.\,°C^{-1}\,h^{-1}$), T is 2-m air temperature (C), $RTMF$ is the radiation temperature melt factor ($mm\,w.e.\,W^{-1}\,m^2\,°C^{-1}\,h^{-1}$), RMF is the radiation melt factor ($mm\,w.e.\,W^{-1}\,m^2\,h^{-1}$), α is albedo (dimensionless), and $I_{o/p}$ is incident global radiation. The subscripts for this term relate to the fact that we run models B and C using global radiation measured/parameterized at the glacier AWSs (I_o) and potential, clear-sky radiation (I_p), which is determined for our sites using standard equations of solar geometry (Oke, 1987) and includes the effects of shading, slope and exposition. To facilitate these calculations, topographic information from the Koblet *et al.* (2010) digital elevation model (DEM) for Storglaciären and from the Advanced Spaceborne Thermal Emission and Reflection Radiometer Global DEM for Vestari Hagafellsjökull is used. Similar to Equation (1), models B and C only permit melting when the hourly air temperature is above a threshold, which we assume to be 0 °C.

The albedo required in Equations (2) and (3) is taken directly from observed/prescribed values at the locations of the glacier AWSs. Whilst this likely results in a favourable performance of models B and C, our aim does not include the assessment of empirical schemes for simulating albedo: Using values retrieved from the AWSs enables greater focus on addressing the variability of temperature-index model parameters between weather types. The models are run with an hourly time step, and all the driving meteorological variables are taken from hourly observations made at, or parameterized for, the glacier AWSs (Section on Glacier Melt Rates).

Coefficients are calibrated for five models (three algorithms; B and C are implemented with both observed and clear-sky global radiation). Optimal values are determined using the Nash–Sutcliffe efficiency coefficient (Nash and Sutcliffe, 1970):

$$R^2 = 1 - \sum_{i=1}^{i=h} \frac{\left(M_{ri} - M_{si}\right)^2}{\left(M_{ri} - \overline{M_{ri}}\right)^2} \qquad (4)$$

where M is the melt rate and subscripts r and s denote the reference series (calculated with the SEB models) and melt simulated by the temperature-index model respectively. The overbar in Equation (4) indicates the mean, and h gives the number of melt values for which to evaluate goodness of fit between reference and simulated values. The objective function, $1 - R^2$, is minimized using the Nelder–Mead simplex algorithm to find optimal values for model coefficients. The algorithm is implemented via the Matlab 'fminsearch' function, and Equation (4) is calculated for hourly melt rates.

Temporally variable model coefficients

The core of the technique investigated is to identify meteorologically similar days from spatially coarse reanalysis data and to vary temperature-index model coefficients accordingly. Similarity of weather between days is judged using the PC scores described in Section on Reanalysis Data. For any pair of days ($\mathbf{D}_t$ and $\mathbf{D}_w$), this is quantified according to

$$\delta(\mathbf{D}_t, \mathbf{D}_w) = \sqrt{\sum_{i=1}^{q} (v_{ti} - v_{wi})^2} \quad (5)$$

where v is the vector of PC scores with q dimensions; here, $q = 5$ because the first five PCs were retained to describe daily meteorology. Calculating $\delta(\mathbf{D}t,\mathbf{D}_w)$ means that archived days can be ranked according to their similarity to the prevailing meteorology. This approach underpins the nearest-neighbour resampling techniques often used to synthesize climate series from historical observations (e.g. Young, 1994; Beersma and Buishand, 2003). Here, the method is used to identify periods with similar meteorological conditions to condition temperature-index model parameters.

The utility of this technique is determined through a cross-validation procedure, implemented at each location as follows:

1. For every day, $\delta(\mathbf{D}_t,\mathbf{D}_w)$ is calculated between the present day and all other days from other years. Only days from other years are considered in the application of Equation (5) because a condition of cross-validation schemes is that the simulated data should be independent of that used for calibration (Elsner and Schmertmann, 1994). To avoid autocorrelation within the melt series compromising the cross validation, data from the same year as the day being simulated are therefore excluded from the fitting procedure.
2. The $\delta(\mathbf{D}_t,\mathbf{D}_w)$ measure is used to rank all days evaluated in step one.
3. Using the reference melt series and Equation (4), all coefficients for each temperature-index model are calibrated on the k most similar days to the present.
4. The present day's melt is simulated at hourly resolution using the respective algorithms and the coefficient estimates obtained in step three.

Thus, all parameters for the five models are calculated N times for every location, using the k most meteorologically similar days for calibration.

The choice of k in the algorithm is evidently important. Previous research employing nearest-neighbour resampling suggests that setting $k = n^{1/2}$ yields favourable results, provided that the number of potential neighbours, n, is at least 100 and $q \leq 6$ (Lall and Sharma, 1996). In our cross-validation scheme, n is simply the number of days that are compared with each day on which melt is simulated, so our data satisfy these criteria (n is 552, 736 and 372 at VH 500, VH 1100 and Storglaciären respectively). Parameter k is, therefore, set to the nearest integer of $n^{1/2}$ in the algorithm (23, 27 and 19 respectively).

Model A requires that only days of the same glacier surface type are considered for calibrating model coefficients, so at each site, only such days are evaluated for meteorological similarity in step one of our algorithm. This means that n is dynamic for this model, depending on the number of days of comparable surface type in the other years (identified from the albedo record: Figure 4). Because snow cover is rare at two of our sites (VH 500 and Storglaciären), this sometimes results in n falling well below the 100-day threshold outlined previously, so the choice of k may be inappropriate for these days. However, this effect is anticipated to have a minimal

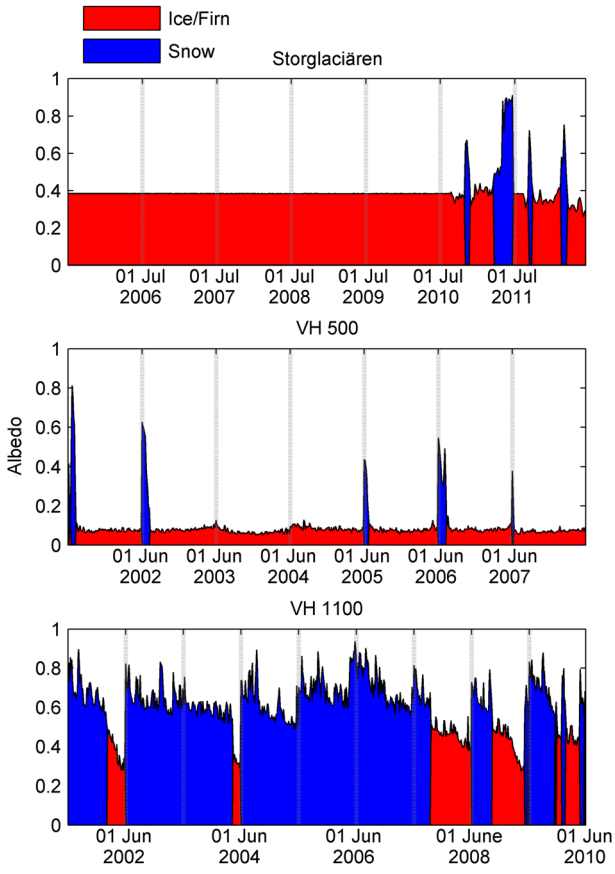

Figure 4. Daily albedo observed at the glacier AWSs. Red indicates ice at VH 500 and Storglaciären and firn at VH 1100; blue illustrates periods of snow cover for all locations. These surface types were identified using albedo thresholds of 0.38, 0.15, and 0.5 at Storglaciären, VH 500, and VH 1100 respectively. The thresholds were prescribed after manual examination of the albedo record at each location [refer to Matthews (2013) for further information]. The vertical grey lines separate successive periods of observation (June–August on Vestari Hagafellsjökull and July–August on Storglaciären). The stability of albedo at Storglaciären prior to 2010 reflects the fact that albedo was not measured on the glacier prior to this year, so it was instead prescribed (Section on Glacier Melt Rates)

effect on simulations as the majority of the series at these locations (94 and 89% respectively) is modelled with coefficients estimated for days that satisfy the threshold for prescribing k (i.e. those days not designated as snow).

The cross-validation procedure is also run to estimate the skill of the models when coefficients do not reflect weather-type variations. This means that, for every day, coefficients are simply calibrated using all data in the remaining years, irrespective of meteorological similarity. This results in coefficient estimates that only vary between years. For each of the models, we therefore have two melt series generated via the cross-validation procedure: one simulated with coefficients that vary daily with the prevailing synoptic weather types (hereafter the '*WT*' series) and the other simulated with coefficients that only vary interannually (hereafter the '*S*' series). Evaluating both series' correspondence with the reference melt record (Equation (4)), and comparing performance, provides insight into the value added by the weather-type calibration routine.

The significance of any improvement in skill is assessed using a bootstrap simulation, implemented by selecting observations from both series on m randomly chosen days and evaluating their correspondence with reference series on these days. The bootstrap is run with 10^4 samples, and m is set to the number of days in 1 year's melt record at our study glaciers (92 and 62 days at Vestari Hagafellsjökull and Storglaciären respectively). For each of the models, counting the number of times the *WT* series exhibits greater correspondence with the reference melt record than the *S* series (according to Equation (4)) and dividing this count by 10^4 provides an estimate of the probability of not obtaining an increase in seasonal melt simulation using our approach (Willmott *et al*., 1985). We evaluate all models in terms of their ability to simulate both hourly and daily melt totals.

The cross-validation procedure also generates an N-member ensemble of coefficient estimates for each model at each location. Examining these series in relation to the prevailing glacier meteorology provides a diagnostic of processes behind the model coefficients' variability. This is pursued by correlating the daily coefficient values for each of the five models with daily mean meteorological variables and components of the SEB determined at the AWSs. Correlating model coefficients between locations on Vestari Hagafellsjökull also permits insight into the spatial coherence of their variability in response to synoptic weather types.

RESULTS

Model performance

The results of applying the five models are illustrated in Figures 5 and 6, while performance measures for each site are shown in Table VI. The best performances are registered by the ETI models forced with observed global radiation, and Model C generally scores higher R^2 values than Model B. Model A performs relatively poorly at hourly resolution but performs better relative to ETI models when evaluated at daily resolution. Model B suffers the greatest reduction in skill, and the range in performance between locations is also larger for all models when examined at daily timescales. Irrespective of whether hourly or daily melt rates are examined, the performance of the models is on average best at Storglaciären and worst at VH 500.

Across all models, the *WT* series exhibit greater correspondence with reference melt series, registering median improvements (with respect to the *S* series) of 7.3 and 23.6% in the simulation of hourly and daily melt rates respectively. There is no clear pattern with regard to which model registers the most improvement when calibrated with respect to weather types, but there is a general tendency for the magnitude of improvement to be inversely related to performance of the unmodified temperature-index model (Figure 7).

An example of the output from the bootstrap procedure is shown in Figure 8, and the full results are recorded in Table VI. The probability of not obtaining an enhancement in a seasonal melt simulation using the weather-type approach to calibrate model coefficients is low ($p < 0.05$) for all models at all locations.

Model coefficients

Mean coefficient values obtained for each model during cross validation, and their respective coefficients of variation ($\sigma/\mu * 100$), are shown in Table VII. Estimates of $MF_{snow/ice}$ (Model A) range between 0.28 and 0.685 mm w.e. $°C^{-1}\,h^{-1}$ for the *WT* and *S* series, with higher values almost universally observed for ice surfaces. These estimates are within the bounds reported in the literature (e.g. Hock, 2003). For the ETI models, *TMF* values between 0.107 and 0.231 mm w.e. $°C^{-1}\,h^{-1}$ are observed, and values of *RMF* and *RTMF* fall between 0.0010 (*RTMF*: mm w.e. $W^{-1}\,m^2\,°C^{-1}\,h^{-1}$) and 0.0105 (*RMF*: mm w.e. $W^{-1}\,m^2\,h^{-1}$). These values are also in general agreement with those reported in the literature (Hock, 1999; Carturan *et al*., 2012; Irvine-Fynn *et al*., 2014).

Between weather types, *TMF* is the most variable coefficient, whilst *RMF* in Model C is the least variable, particularly when this model is forced by observed global radiation. For both ETI models, radiation coefficients are more stable when the observed flux is used in the cross-validation procedure. Figure 9 highlights the variability of coefficients around the globally optimum coefficient values observed during the cross-validation procedure for the ETI models (Figure 9 caption). Model B generally exhibits greater departure from these optimum values, highlighting the need for a larger adjustment of ETI model values to

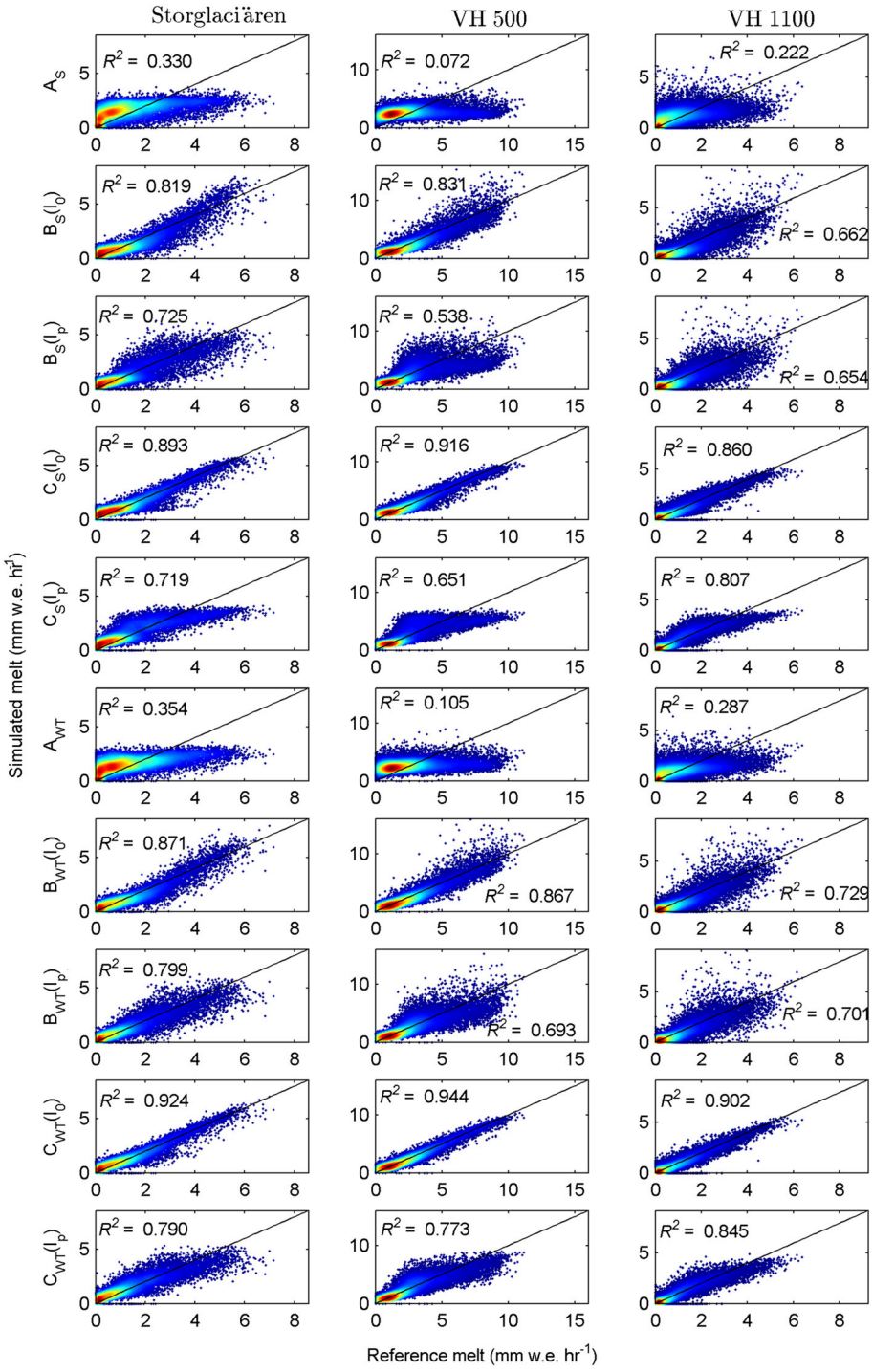

Figure 5. Comparisons between reference melt series and the melt simulated by the temperature-index models at hourly resolution. The locations are separated by columns, and model variants are differentiated by row. Rows are labelled such that the first letter corresponds to the model name, and the subscript indicates whether static (S) or weather-type-dependent (WT) model coefficients were applied in the model being evaluated. The bracketed terms in the *y*-axis labels denote whether the ETI models were forced with observed or potential, clear-sky global radiation (Section on Temperature-Index Models). The relative density of points in the plots is indicated by shading (red = high density; blue = low density)

account for the prevailing weather compared with Model C. Figure 9 also demonstrates the interdependence of temperature and radiation parameters in the ETI models that is evident for the entire dataset (shown by the slope in the contour field), but that is particularly apparent between weather types (shown by the linear relation evident in the scatter plot). Only when Model C is driven by observed global radiation do the temperature and radiation coefficients

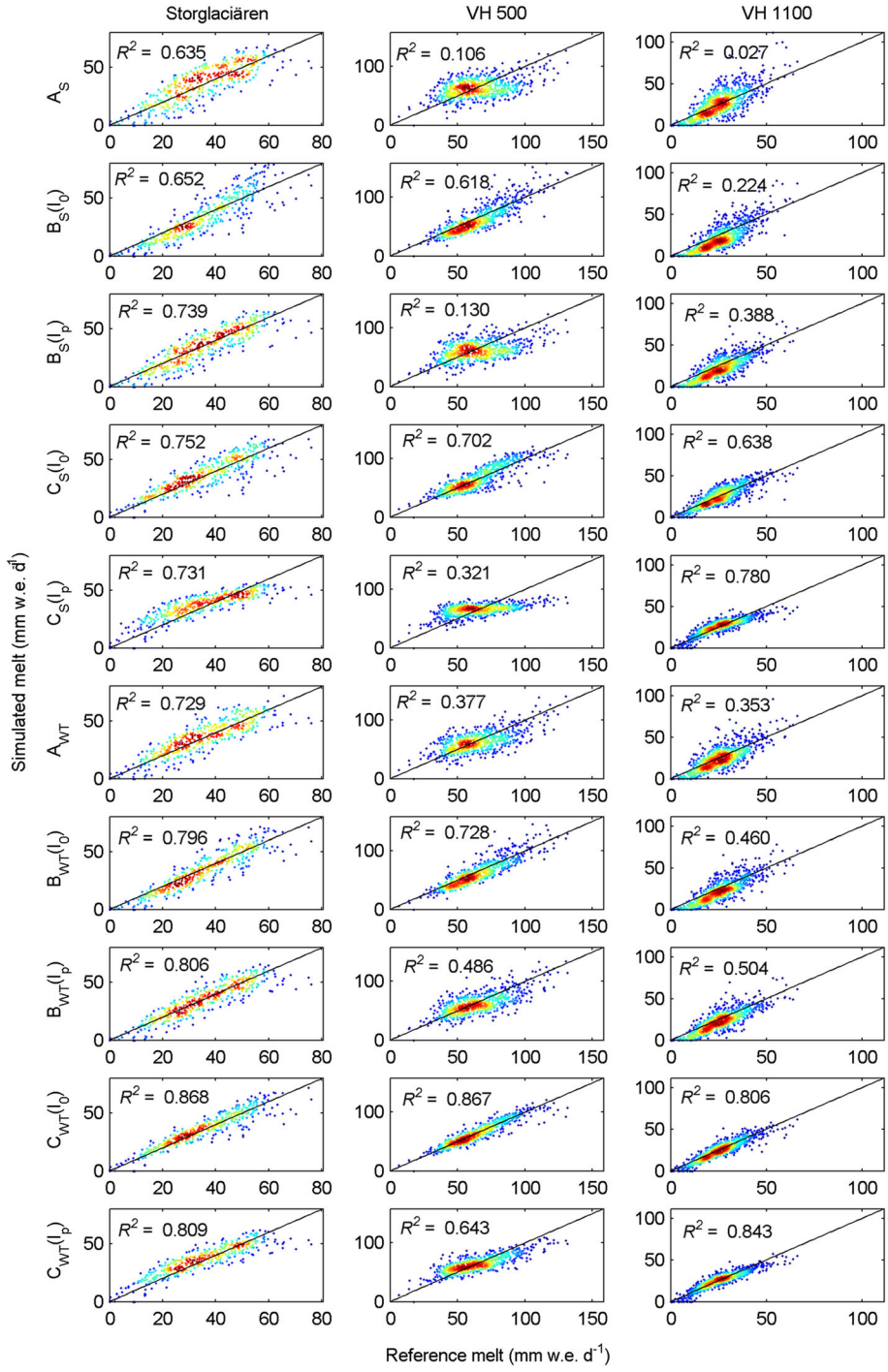

Figure 6. Comparisons between reference melt series and the melt simulated by the temperature-index models at daily resolution. Refer to the caption of Figure 5 for further information

appear to vary independently between weather types, which results from the stability of the *RMF* term. Models driven by potential global radiation show the most pronounced interdependence of model coefficients between weather types.

The cause of variability in model coefficients between weather types was explored by correlating values obtained for each model in the cross-validation procedure with daily mean values of the prevailing meteorology/SEB components for the locations of the AWSs (Figure 10). *TMF* values exhibit consistency in their correlations between models and locations, being positively correlated with the turbulent and longwave heat fluxes and negatively correlated with the shortwave heat flux. Consistent with

Table VI. Performance measures for the temperature-index models

		Hourly					Daily				
		R^2					R^2				
	Model	*S*	*WT*	ΔR^2 (*WT* − *S*)	ΔR^2 as % of R^2 (*S*)	*p* (%)	*S*	*WT*	ΔR^2 (*WT* − *S*)	ΔR^2 as % of R^2 (*S*)	*p* (%)
Storglaciären	A	0.330	0.354	0.024	7.3	0.6	0.635	0.729	0.094	14.8	1.9
	B (I_o)	0.819	0.871	0.052	6.3	0.0	0.652	0.796	0.145	22.2	0.1
	B (I_p)	0.725	0.799	0.074	10.2	0.0	0.739	0.806	0.068	9.2	1.2
	C(I_o)	0.893	0.924	0.031	3.5	0.0	0.752	0.868	0.116	15.4	0.0
	C(I_p)	0.719	0.790	0.071	9.9	0.0	0.731	0.809	0.077	10.6	0.3
VH 500	A	0.072	0.105	0.034	47.3	0.2	0.106	0.377	0.271	255.4	0.1
	B (I_o)	0.831	0.867	0.037	4.4	0.0	0.618	0.728	0.111	18.0	0.3
	B (I_p)	0.538	0.693	0.155	28.9	0.0	0.130	0.486	0.356	274.9	0.0
	C(I_o)	0.916	0.944	0.029	3.1	0.0	0.702	0.867	0.166	23.6	0.0
	C(I_p)	0.651	0.773	0.122	18.8	0.0	0.321	0.643	0.322	100.5	0.0
VH 1100	A	0.222	0.287	0.065	29.5	1.1	0.027	0.353	0.326	1207.0	1.6
	B (I_o)	0.662	0.729	0.067	10.1	0.1	0.224	0.460	0.237	105.8	0.4
	B (I_p)	0.654	0.701	0.047	7.2	0.5	0.388	0.504	0.116	29.9	0.4
	C(I_o)	0.860	0.902	0.043	5.0	0.0	0.638	0.806	0.168	26.4	0.0
	C(I_p)	0.807	0.845	0.038	4.7	0.0	0.780	0.843	0.064	8.2	0.1
	Median	0.719	0.790	0.047	7.3	0.0	0.633	0.728	0.145	23.6	0.1

The *S* series (modelled with coefficients which are static) and the *WT* series (modelled with coefficients that are conditioned on synoptic weather types) are compared with the reference melt rates (generated with the SEB models) at hourly and daily resolution (left-hand and right-hand-side columns respectively). ΔR^2 gives the difference in Nash–Sutcliffe efficiency coefficient (as indicated in brackets), and R^2 (*S*) gives this improvement as a % of the R^2 for the *S* series. *p* gives the bootstrapped probability of not obtaining an improvement in annual melt simulation using the weather-type calibration routine.

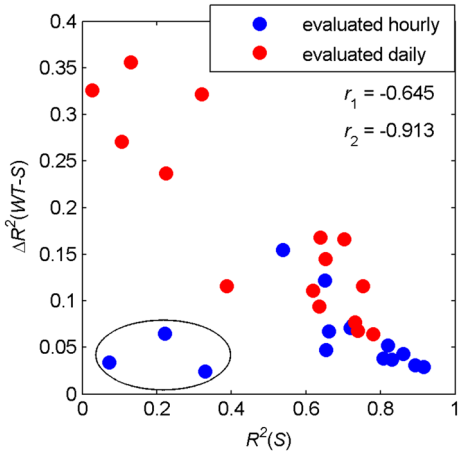

Figure 7. The R^2 achieved by the unmodified temperature-index models in the cross-validation procedure (i.e. those models with static model coefficients) *versus* the improvement in R^2 (R^2 for the *WT* series minus R^2 for the *S* series) attained when coefficients are calibrated with respect to weather types. The ellipse bounds the results from Model A when evaluated at hourly resolution: r_1 and r_2 give the Pearson product-moment correlations between the series when these points are included and omitted from the correlation analysis respectively: Both *r*-values are significant at $p < 0.05$ (two-tailed *t*-test)

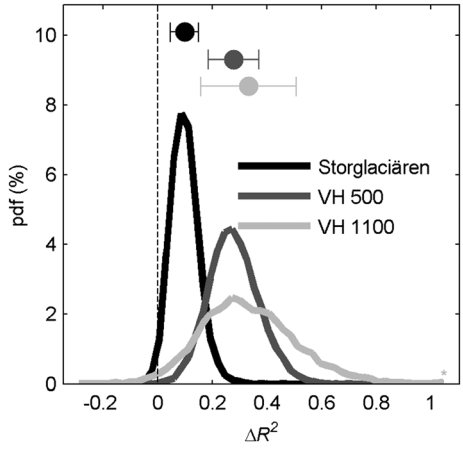

Figure 8. An example of the results from the bootstrap simulation described in Section on Temporally Variable Model Coefficients, which assesses the significance of the improvement in temperature-index model performance when coefficients are varied as a function of weather type. Displayed are the results of evaluating Model A at daily resolution. The circles and bars above the probability density functions denote the means and standard deviations respectively

these associations, Figure 10 indicates that *TMF* coefficients exhibit the strongest positive correlations with cloud cover and vapour pressure and weaker positive correlations with air temperature and wind speed.

RMF and *RTMF* exhibit similar correlations with the prevailing meteorology and SEB between locations, which are somewhat opposite in sign to the those observed for *TMF*s. Both *RMF* and *RTMF* correlate positively with the shortwave heat flux and negatively with the longwave heat flux and cloud cover. These correlations are typically

Table VII. Mean coefficient values (μ) and their coefficients of variation ($c_v = \sigma/\mu * 100$) for the temperature-index models used to simulate the *S* and *WT* series

	Storglaciären		VH 500		VH 1100	
Coefficient	μ	c_v	μ	c_v	μ	c_v
			***S* Series**			
MF_{snow}(A)	0.285	1.2	0.450	2.5	0.493	1.2
MF_{ice}(A)	0.290	3.6	0.523	1.0	0.593	3.0
$TMF(B_0)$	0.135	2.7	0.214	1.6	0.195	1.7
$TMF(B_p)$	0.124	3.3	0.231	1.4	0.179	2.0
$TMF(C_0)$	0.132	2.8	0.228	1.1	0.171	1.8
$TMF(C_p)$	0.143	2.0	0.225	2.1	0.182	1.4
$RTMF(B_0)$	0.0012	0.8	0.0019	1.2	0.0026	1.1
$RTMF(B_p)$	0.0010	2.7	0.0012	2.4	0.0027	1.4
$RMF(C_0)$	0.0087	0.8	0.0101	0.3	0.0089	0.5
$RMF(C_p)$	0.0065	2.3	0.0071	1.5	0.0083	0.7
			***WT* Series**			
MF_{snow}(A)	0.317	23.8	0.448	5.1	0.549	17.3
MF_{ice}(A)	0.300	19.0	0.530	15.5	0.685	21.8
$TMF(B_0)$	0.115	32.6	0.183	39.7	0.167	72.8
$TMF(B_p)$	0.113	32.5	0.209	27.0	0.160	57.7
$TMF(C_0)$	0.107	36.8	0.193	34.0	0.130	71.3
$TMF(C_p)$	0.133	23.1	0.208	26.7	0.159	50.0
$RTMF(B_0)$	0.0014	25.5	0.0020	15.9	0.0031	23.0
$RTMF(B_p)$	0.0012	41.3	0.0013	41.9	0.0031	27.9
$RMF(C_0)$	0.0092	6.9	0.0105	3.9	0.0093	6.7
$RMF(C_p)$	0.0065	34.4	0.0073	33.4	0.0084	20.0

The units for the coefficients are as follows: $MF_{snow/ice}$ = mm w.e. $°C^{-1} h^{-1}$, *TMF* = mm w.e.$°C^{-1} h^{-1}$; *RTMF* = mm w.e. $W^{-1} m^2 °C^{-1} h^{-1}$, and *RMF* = mm w.e. $W^{-1} m^2 h^{-1}$.

stronger for the models forced with potential global radiation, particularly for *RMF*. Correlations for $MF_{snow/ice}$ show a high degree of similarity to those recorded for the radiation melt factors, especially those observed for *RTMF*. MF_{snow} at VH 500 is an exception, exhibiting correlations very similar to those obtained for the *TMF*s at this location.

The difference in correlations with the SEB and prevailing meteorology observed for MF_{snow} between elevations on Vestari Hagafellsjökull results in little temporal correspondence between these coefficient estimates (Figure 11). For all the other coefficients, their daily values are positively correlated between elevations. The strongest agreement is for the *TMF* coefficients. For both *RMF* and *RTMF*, those models forced by potential global radiation are more strongly correlated between locations.

DISCUSSION

Model performance and coefficient variability

At all locations, and for all models, our weather-type approach to calibrating parameters significantly improved melt simulations, with the greatest enhancements apparent for daily melt totals. This is explained by the fact that model coefficients in the algorithm described earlier (Section on Temporally Variable Model Coefficients) vary on a daily timescale, depending on synoptic weather type. Thus, subdaily variability in coefficients cannot be accounted for. The observation that weather-type conditioning resulted in larger improvements for models more limited in initial skill demonstrates greater benefit of applying our modelling approach where temperature-index methods are more limited in their ability to capture processes of surface energy exchange.

Correlations between parameters from the *WT* series and the prevailing meteorology provide insight to this value added by weather-type conditioning. *TMF* coefficients in all models were found to be correlated most strongly with latent and longwave heat fluxes. This can be understood through consideration of the SEB, as these energy components are related to air temperature in a non-linear way, through the Clausius Clapeyron and Stefan Boltzmann equations respectively. The former relation also explains the positive correlations observed between *TMF* and vapour pressure at all locations. The strong positive association with cloud cover is in agreement with Carenzo *et al.* (2009). This can be understood through a priori SEB considerations, as the sensitivity of the longwave heat flux to air temperature would be expected to rise as the apparent emissivity of the atmosphere increases (*cf* Sedlar and Hock, 2009).

Both *RMF* and *RTMF* exhibit the strongest positive correlations with the net shortwave heat flux, and this too is in agreement with Carenzo *et al.* (2009). Additionally, these coefficients are generally correlated more strongly with the prevailing meteorology/SEB when models are forced with potential global radiation. This is most notable for correlations with cloud cover and the longwave heat flux (themselves strongly co-linear at each location: minimum $r = 0.82$ at Storglaciären). These stronger correlations reflect the fact that no provision is made for temporal variability in atmospheric transmissivity for the models forced with potential global radiation, so this information must be included implicitly in the value of the scalars *RMF* and *RTMF*. This mechanism also provides an explanation for the reduced variability of the radiation factors in models forced with observed global radiation.

Compared with *RMF*, *RTMF* is more variable between weather types irrespective of whether observed or global radiation is used to drive the models. Model B therefore exhibits a higher sensitivity to changes in the prevailing meteorology, consistent with previous interpretations of ETI model errors that have applied this algorithm (Konya *et al.*, 2004; Carturan *et al.*, 2012; Irvine-Fynn *et al.*, 2014). This is possibly an artefact of the physically unrealistic scaling of the net shortwave heat flux by air temperature (Pellicciotti *et al.*, 2005; Irvine-Fynn *et al.*, 2014). This, coupled with the lower model skill generally exhibited by Model B relative to Model C, even when variable weather

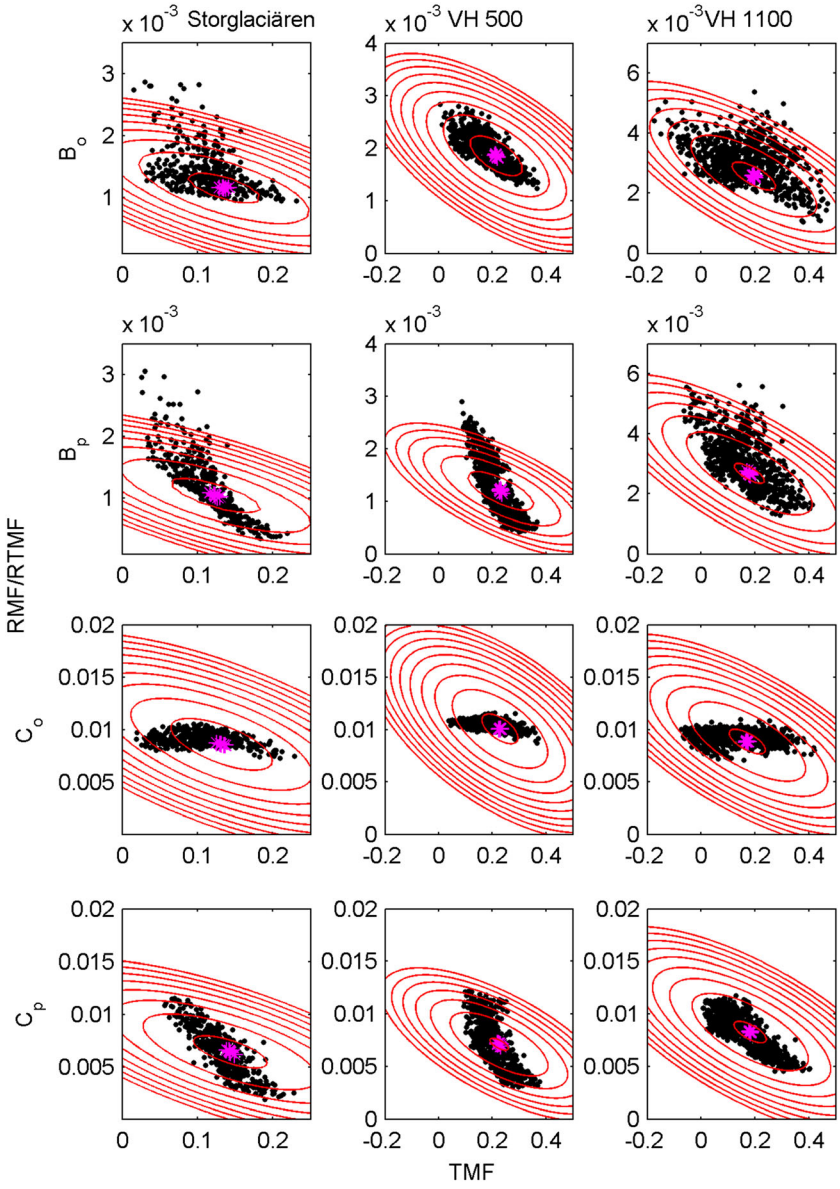

Figure 9. The response surface for the ETI model coefficients is given by the contour field. This was generated by simultaneously varying coefficients over a wide range and calculating R^2 for each resulting combination – performed using all available data to train the models and evaluate their performance (i.e. off-line from the cross-validation procedure). The black and magenta scatter plots indicate the calibrated coefficient values obtained from the cross-validation procedure for the models with weather-type-dependent and static model coefficients respectively. Note that the *y*-axis represents either the *RTMF* or *RMF* coefficient, depending on the model (models B and C respectively)

types were provisioned for, makes the additive structure of the Pellicciotti *et al*. (2005) algorithm the most attractive of the methods investigated for melt simulation at these glaciers.

Whilst Model A could not be expected to match the performance of the ETI models, there is additional interest in the meteorological controls on the *MF* given its widespread use for glacier melt modelling under climate change (e.g. Raper and Braithwaite, 2006; Radić and Hock, 2011). MF_{ice} exhibited meteorological dependence similar to those observed for the radiation melt factors of models B and C, with positive and negative correlations apparent for the shortwave and temperature-dependent heat fluxes respectively. This is consistent with the net shortwave heat flux being the dominant source of melt energy at all locations (Table V), agreeing with the controls outlined by Hock (2003) and suggesting a relationship similar to that proposed by Irvine-Fynn *et al*. (2014). MF_{snow} did not display the same level of agreement with the radiation melt factors in regard to its dependence on the prevailing weather, likely because of the reduced importance of net shortwave heat in the SEB as snow cover lowers surface albedo considerably (Figure 4).

The value added to model skill by dynamic model coefficients conditioned on weather types can be attributed

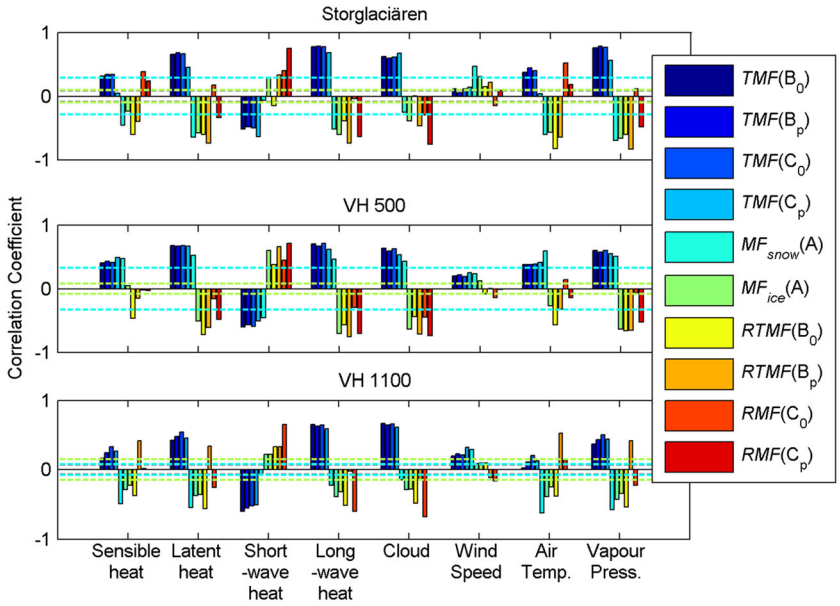

Figure 10. Pearson product-moment correlation coefficients (r) between the value of the temperature-index model coefficients calibrated for each of the weather types during the cross-validation procedure and the mean daily meteorological/energy balance conditions at the location of the glacier AWSs for the day that the coefficients were calibrated for. Note that the dotted lines indicate the respective critical values of r to reject the null hypothesis that $r = 0$ according to a t-test. Different critical values reflect the different samples sizes because of surface types (Model A), which are colour coded to match the relevant legend entries for this model. Critical r values for models B and C are plotted but are obscured by the lower magnitude critical values plotted for the snow/ice surfaces

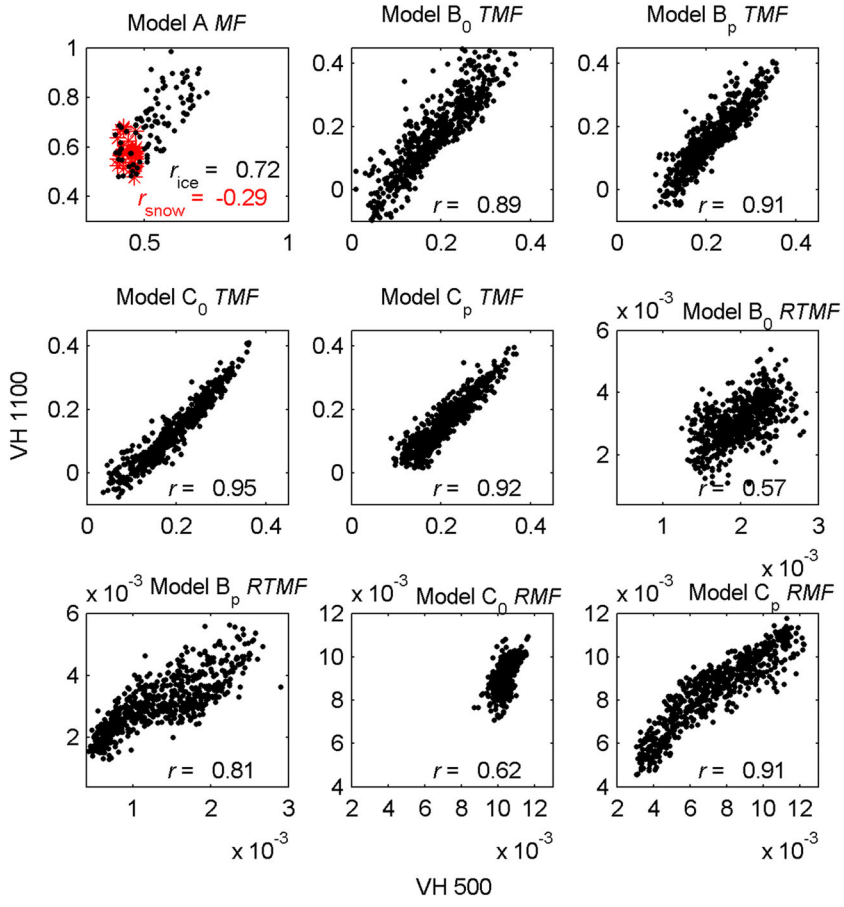

Figure 11. Correlations for model coefficients calibrated at different elevations on Vestari Hagafellsjökull between weather types. All correlations are significant at $p < 0.05$ according to a two-tailed t-test, except the correlation observed for MF_{snow}, which has a p-value of 0.08

to reduction in high-frequency error. Changes in the sensitivity of the temperature-dependent heat fluxes to air temperature, for example, that reflect the effects of variable temperatures, humidity, thermal emissivities and wind speeds can be provisioned for by varying *TMF*. The variable sensitivity of the SEB to net shortwave heat, which varies principally with the magnitude of the incident flux, can also be adjusted, as can the value of the *MF*, which exhibits dependence similar to the radiation coefficients in the ETI models. Conditioning by weather types accounts for variations in these parameters by invoking the analogue principle (Kuhn, 1993), which simply assumes that similarity in synoptic weather between days translates to similar on-glacier meteorology and, consequently, similar model coefficients being appropriate. The processes driving parameter variability do not need to be addressed explicitly.

This approach to dynamic parameter allocation may also provide a more conceptually robust means of integrating climate variability into melt simulations. In order to limit errors from static model coefficients to acceptable levels, average weather must stay constant in time, yet this condition must be considered unlikely to be satisfied. Studies of atmospheric circulation in the mid-latitudes and high latitudes during the last century, for example, have demonstrated considerable non-stationarity in the frequency of air masses/weather types (Bárdossy and Caspary, 1990; Kalkstein *et al*., 1990; Wilby 1997). In addition, large changes in atmospheric circulation have been noted recently for the glacierized margin of the North Atlantic (Fettweis *et al*., 2011, 2013; Hanna *et al*., 2012). Whatever their cause, failure to accommodate changes in the mean weather resulting from variable atmospheric circulation undermines the assumption of static model coefficients. Use of transient model parameters as demonstrated here offers an improved approach to accommodate variability in the frequency of weather types in model calibration explicitly.

It must also be recognized that weather types are prone to differential rates of warming under a changing climate (e.g. Kalkstein *et al*., 1990). In the northern hemisphere, for example, high-latitude air masses are likely to warm most rapidly because of Arctic amplification (Holland and Bitz, 2003; Serreze *et al*., 2009). If static temperature sensitivities are assumed, large errors in simulated melt will manifest if rapid warming occurs in those weather types with sensitivities furthest from the average calibrated coefficients that quantify this association. This potential source of error can be traced by analysing the time-varying parameters associated with individual weather types.

Study limitations and transferability of the modelling approach

In interpreting the improvement offered by our weather-type approach to parameter calibration, it is important to consider that our reference melt series are generated by SEB models, and these are prone to uncertainty, particularly with regard to estimation of the turbulent heat fluxes (Hock, 2005). Our bootstrapped test of the enhancement provided by the weather-type melt models makes no provision for the fact that their performance is not assessed relative to a 'true' melt rate, and thus, the significance of our improvement should be interpreted with caution. This is especially true at Storglaciären, where most of the reference melt series was generated using parameterized TRS data. However, we note that the skill in simulating melt exhibited by the weather-type-dependent models is similar when evaluated relative to the reference melt series in 2011 (where almost all data are taken from glacier AWS observations), as it is in other years (when mainly TRS data are used: Table VIII). Thus, whilst the extent of the uncertainty introduced by the parameterized series remains somewhat unquantified, this assessment at least provides confidence that the improvement in simulation performance achieved at this location does not depend on the use of these off-glacier data.

A simplification applied in the modelling procedure was to use measured values of albedo to prescribe surface types (Model A) and to obtain the net global radiation (Models B and C). It is considered unlikely that this results in *bias* in the model comparison, as this information would seem equally important for both the weather-type and static models. This issue does, however, raise an interesting point

Table VIII. The relative skill of the temperature-index models with static and weather-type-dependent coefficients for different periods at Storglaciären

	2005–2010			2011		
	R^2			R^2		
Model	*WT*	*S*	ΔR^2 (*WT* − *S*)	*WT*	*S*	ΔR^2 (*WT* − *S*)
			Hourly			
A	0.333	0.356	0.023	0.299	0.335	0.037
B (I_o)	0.815	0.870	0.055	0.822	0.851	0.030
B (I_p)	0.726	0.798	0.073	0.685	0.773	0.088
C(I_o)	0.891	0.921	0.031	0.888	0.923	0.035
C(I_p)	0.722	0.789	0.067	0.675	0.776	0.100
Mean	0.697	0.747	0.050	0.674	0.732	0.058
			Daily			
A	0.522	0.624	0.102	0.630	0.783	0.153
B (I_o)	0.519	0.739	0.220	0.809	0.848	0.039
B (I_p)	0.670	0.766	0.096	0.800	0.843	0.043
C(I_o)	0.700	0.842	0.143	0.822	0.913	0.091
C(I_p)	0.707	0.782	0.076	0.715	0.830	0.115
Mean	0.623	0.751	0.127	0.755	0.843	0.088

Refer to Table VI and the text in Section on Study Limitations and Transferability of the Modelling Approach for further information.

regarding the transferability of our approach. The SEB is a function of the interaction between the boundary layer meteorology and the glacier surface. Changing glacier surface conditions (e.g. albedo, surface roughness and debris cover) introduce variability to melt rates independent of the prevailing weather that cannot be captured using the weather-type approach. Hence, on glaciers where temporal variability of surface properties is pronounced, more limited benefit might be realized by calibrating parameters with respect to weather types.

While our approach offers improved simulations at the point scale, distributing dynamic coefficients across the glacier adds further uncertainty to the modelling procedure. However, considering that variation of the transient model parameters was strongly coherent between elevations on Vestari Hagafellsjökull, the evidence suggests that our approach may be extended to glacierwide simulations if judicious placement of AWSs is accompanied by interpolation of model parameters over the glacier.

The temporal transferability of our modelling approach also demands consideration. Changes in the internal structure of weather types would limit the advantage of our calibration method. If climate change manifests as weather types without precedent during calibration, then this strategy will be compromised. By the same reasoning, it is also likely that our weather-type approach to calibration will be most useful for glaciers where long records of observation are available and the information content of calibration data is maximized (Van den Dool, 1994). Variations in the SEB that may occur with time and that are independent of the prevailing weather (e.g. changes in glacier hypsometry: Braithwaite, 2008) can of course not be accounted for with our calibration strategy either.

CONCLUSIONS

This study evaluated the utility of varying temperature-index model parameters to reflect changes in prevailing weather during melt simulations. Our results indicate that using spatially coarse reanalysis data to define periods of meteorological similarity for calibrating models significantly enhances the skill of three algorithms commonly used to simulate site-specific glacier melt rates.

The approach also provides insight to the meteorological and energetic controls of model coefficients. Changes in parameter values between weather types were consistent with expectations from physical considerations of the SEB. Future work should further explore climatological controls on temperature-index model parameters, with a view to determine the transferability of our approach to other glaciers or to spatially distributed modelling approaches across large and/or data-sparse catchments.

ACKNOWLEDGEMENTS

Funding from Natural Environment Research Council (award NER/B/S/2001/00851), the Royal Society (award RG062190 and TG092060) and the Royal Geographical Society (Postgraduate Research Award, received by T. Matthews) is gratefully acknowledged. Conscientious reviewing by an anonymous referee and diligent editing from Conor Murphy improved an earlier version of the manuscript.

REFERENCES

Andreas EL. 1987. A theory for the scalar roughness and the scalar transfer coefficients over snow and sea ice. *Boundary-Layer Meteorology* **38**: 159–184. DOI: 10.1007/BF00121562.

Arendt A, Sharp MJ. 1999. Energy balance measurements on a Canadian high arctic glacier and their implications for mass balance modeling. *IAHS Publication* **256**: 165–172.

Bárdossy A, Caspary H. 1990. Detection of climate change in Europe by analyzing European atmospheric circulation patterns from 1881 to 1989. Theoretical and Applied *Climatology* **42**: 155–167. DOI: 10.1007/BF00866871.

Beersma JJ, Buishand TA. 2003. Multi-site simulation of daily precipitation and temperature conditional on the atmospheric circulation. *Climate Research* **25**: 121–133. DOI: 10.3354/cr025121

Beljaars ACM, Holtslag AAM. 1991. Flux parameterization over land surfaces for atmospheric models. *Journal of Applied Meteorology* **30**: 327–341. DOI: 10.1175/1520-0450(1991)030<0327:FPOLSF>2.0.CO;2.

Bower D, McGregor GR, Hannah DM, Sheridan SC. 2007. Development of a spatial synoptic classification scheme for Western Europe. *International Journal of Climatology* **27**: 2017–2040. DOI: 10.1002/joc.1501.

Braithwaite RJ. 1995. Positive degree-day factors for ablation on the Greenland ice sheet studied by energy balance modeling. *Journal of Glaciology* **41**: 153–160.

Braithwaite R. 2008. Temperature and precipitation climate at the equilibrium-line altitude of glaciers expressed by the degree-day factor for melting snow. *Journal of Glaciology* **54**: 437–444. DOI: 10.3189/002214308785836968.

Carenzo M, Pellicciotti F, Rimkus S, Burlando P. 2009. Assessing the transferability and robustness of an enhanced temperature-index glacier-melt model. *Journal of Glaciology* **55**: 258–274. DOI: 10.3189/002214309788608804.

Carturan LF, Cazorzi G, Fontana D. 2012. Distributed mass-balance modelling on two neighbouring glaciers in Ortles-Cevedale, Italy, from 2004 to 2009. *Journal of Glaciology* **58**: 467–486. DOI: 10.3189/2012jog11j111.

Cazorzi F, Fontana GD. 1996. Snowmelt modelling by combining air temperature and a distributed radiation index. *Journal of Hydrology* **181**: 169–87. DOI: 10.1016/0022-1694(95)02913-3.

Daly SF, Davis R, Ochs E, Pangburn T. 2000. An approach to spatially distributed snow modelling of the Sacramento and San Joaquin basins, California. *Hydrological Processes* **14**: 3257–3271. DOI: 10.1002/1099-1085(20001230)14:18<3257::AID-HYP199>3.0.CO;2-Z.

Dee DP, Uppala SM, Simmons AJ, Berrisford P, Poli PK, Kobayashi S, Andrae U, Balmaseda MA, Balsamo G, Bauer P, Bechtold P, Beljaars ACM, Van de Berg L, Bidlot J, Bormann N, Delsol C, Dragani R, Fuentes M, Geer AJ, Haimberger L, Healy SB, Hersbach H, Hólm EV, Isaksen L, Kållberg P, Köhler M, Matricardi M, Mc Nally AP, Monge-Sanz BM, Morcrette J, Park B, Peubey C, de Rosnay P, Tavolato C, Thépaut J, Vitart F. 2011. The ERA-Interim reanalysis: configuration and performance of the data assimilation system. *Quarterly Journal of the Royal Meteorological Society* **137**: 553–597. DOI: 10.1002/qj.828.

Dobler C, Hagemann S, Wilby RL, Stötter J. 2012. Quantifying different sources of uncertainty in hydrological projections at the catchment scale. *Hydrology and Earth Systems Science* **16**: 4343–4360. DOI: 10.5194/hess-16-4343-2012.

Dyer A. 1974. A review of flux-profile relationships. *Boundary-LayerMeteorology* **7**: 363–372. DOI: 10.1007/BF00240838.

Elsner JB, Schmertmann CP. 1994. Assessing Forecast Skill through Cross Validation. *Weather and Forecasting* **9**: 619–624. DOI: 10.1175/1520-0434(1994)009<0619:AFSTCV>2.0.CO;2.

Fealy R, Sweeney J. 2007. Identification of frequency changes in synoptic circulation types and consequences for glacier mass balance in Norway. *Norsk Geografisk Tidsskrift* **61**: 76–91. DOI: 10.1080/00291950701374328.

Fettweis X, Mabille G, Erpicum M, Nicolay S, Broeke M. 2011. The 1958-2009 Greenland ice sheet surface melt and the mid-tropospheric atmospheric circulation. *Climate Dynamics* **36**: 139–159. DOI: 10.1007/s00382-010-0772-8.

Fettweis X, Hanna E, Lang C, Belleflamme A, Erpicum M, Gallée H. 2013. Brief communication: Important role of the mid-tropospheric atmospheric circulation in the recent surface melt increase over the Greenland ice sheet. *The Cryosphere* **7**: 241–248. DOI: 10.5194/tc-7-241-2013.

Greuell W, Smeets P. 2001. Variations with elevation in the surface energy balance on the Pasterze (Austria). *Journal of Geophysical Research: Atmospheres (1984–2012)* **106**: 31717–31727. DOI: 10.1029/2001JD900127.

Grudd H, Schneider T. 1996. Air temperature at Tarfala research station 1946-1995. *Geografiska Annaler A* **78**: 115–120. DOI: 10.2307/520973.

Guðmundsson S, Björnsson H, Pálsson F, Haraldsson HH. 2009. Comparison of energy balance and degree-day models of summer ablation on the Langjökull ice cap, SW-Iceland. *Jökull* **59**: 1–17.

Hanna E, Jones JM, Cappelen J, Mernild SH, Wood L, Steffen K, Huybrechts P. 2012. The influence of North Atlantic atmospheric and oceanic forcing effects on 1900-2010 Greenland summer climate and ice melt/runoff. *International Journal of Climatology* **33**: 862–880. DOI: 10.1002/joc.3475.

Hock R. 1999. A distributed temperature-index ice- and snowmelt model including potential direct solar radiation. *Journal of Glaciology* **45**: 101–11.

Hock R. 2003. Temperature index melt modelling in mountain areas. *Journal of Hydrology* **282**: 104–115. DOI: 10.1016/s0022-1694(03)00257-9.

Hock R. 2005. Glacier melt: a review of processes and their modeling. *Progress in Physical Geography* **29**: 362–391. DOI: 10.1191/0309133305pp453ra.

Hock R, Holmgren B. 1996. Some aspects of energy balance and ablation of Storglaciären, northern Sweden. *Geografiska Annaler A* **78**: 121–131. DOI: 10.2307/520974.

Hock R, Holmgren B. 2005. A distributed surface energy balance model for complex topography and its application to Storglaciären, Sweden. *Journal of Glaciology* **51**: 25–36. DOI: 10.3189/172756505781829566.

Hodgkins R, Carr S, Pálsson F, Guðmundsson S, Björnsson H. 2012. Sensitivity analysis of temperature-index melt simulations to near-surface lapse rates and degree-day factors at Vestari-Hagafellsjökull, Langjökull, Iceland. *Hydrological Processes* **26**: 3736–3748. DOI: 10.1002/hyp.8458.

Holland MM, Bitz CM. 2003. Polar amplification of climate change in coupled models. *Climate Dynamics* **21**: 221–232. DOI: 10.1007/s00382-003-0332-6.

Irvine-Fynn TDL, Hanna E, Barrand NE, Porter PR, Kohler J, Hodson AJ. 2014. Examination of a physically based, high-resolution, distributed Arctic temperature-index melt model, on Midtre Lovénbreen, Svalbard. *Hydrological Processes* **28**: 134–149. DOI: 10.1002/hyp.9526.

Jonsell U, Hock R, Duguay M. 2013. Recent air and ground temperature increases at Tarfala Research Station, Sweden. *Polar Research* **32**. DOI: 10.3402/polar.v32i0.19807.

Kalkstein LS, Corrigan P. 1986. A synoptic climatological approach for geographical analysis: Assessment of sulphur dioxide concentrations. *Annals of the Association of American Geographers* **76**: 381–395. DOI: 10.1111/j.1467-8306.1986.tb00126.x.

Kalkstein LS, Dunne PC, Vose RS. 1990. Detection of climatic change in the western North American Arctic using a synoptic climatological approach. *Journal of Climate* **3**: 1153–1167. DOI: 10.1175/1520-0442(1990)003<1153:DOCCIT>2.0.CO;2.

Koblet T, Gärtner-Roer I, Zemp M, Jansson P, Thee P, Haeberli W, Holmlund P. 2010. Reanalysis of multi-temporal aerial images of Storglaciären, Sweden (1959-99)—Part 1: Determination of length, area, and volume changes. *The Cryosphere* **4**: 333–343. DOI: 10.5194/tc-4-333-2010.

Konya K, Matsumoto T, Naruse R. 2004. Surface heat balance and spatially distributed ablation modelling at Koryto Glacier, Kamchatka peninsula, Russia. *Geografiska Annaler A* **86**: 337–348. DOI: 10.1111/j.0435-3676.2004.00236.x.

Kuhn M. 1993. Methods of assessing the effects of climatic changes on snow and glacier hydrology. *IAHS Publication* **218**: 135–144.

Lall U, Sharma A. 1996. A nearest neighbor bootstrap for resampling hydrologic time series. *Water Resources Research* **32**: 679–693. DOI: 10.1029/95WR02966.

Lang H, Braun L. 1990. On the information content of air temperature in the context of snow melt estimation. *IAHS Publication* **190**: 347–354.

Maraun D, Wetterhall F, Ireson AM, Chandler RE, Kendon EJ, Widmann M, Thiele-Eich I. 2010. Precipitation downscaling under climate change: Recent developments to bridge the gap between dynamical models and the end user. *Reviews of Geophysics* **48**. DOI: 10.1029/2009RG000314.

Marzeion B, Jarosch AH, Hofer M. 2012. Past and future sea-level change from the surface mass balance of glaciers. *The Cryosphere* **6**: 1295–1322. DOI: 10.5194/tc-6-1295-2012.

Matthews TKR. 2013. Glacier-climate interactions: a synoptic approach. PhD thesis. Available from: https://dspace.lboro.ac.uk/2134/12558.

Meehl GA, Stocker TF, Collins WD, Friedlingstein P, Gaye AT, Gregory JM, Kitoh A, Knutti R, Murphy JM, Noda A, Raper SCB, Watterson IG, Weaver AJ, Zhao ZC. 2007. Global Climate Projections. In *Climate Change 2007: The Physical Science Basis Contribution of Working Group I to the Fourth Assessment Report of the Intergovernmental Panel on Climate Change*, Solomon S, Qin D, Manning M, Chen Z, Marquis M, Averyt KB, Tignor M, Miller HL (eds). Cambridge University Press: Cambridge, United Kingdom and New York, NY, USA.

Müller F, Keeler CM. 1969. Errors in short-term ablation measurements on melting ice surfaces. *Journal of Glaciology* **8**: 91–105.

Munro DS. 1990. Comparison of melt energy computations and ablatometer measurements on melting ice and snow. *Arctic and Alpine Research* **22**: 153–162. DOI: 10.2307/1551300.

Nash JE, Sutcliffe JV. 1970. River flow forecasting through conceptual models. Part 1. A discussion of principles. *Journal of Hydrology* **10**: 282–290. DOI: 10.1016/0022-1694(70)90255-6.

Oke TR. 1987. *Boundary layer climates*, 2nd edn. Routledge Press: London.

Paulson CA. 1970. The mathematical representation of wind speed and temperature profiles in the unstable atmospheric surface layer. *Journal of Applied Meteorology* **9**: 857–861. DOI: 10.1175/1520-0450(1970)009<0857:TMROWS>2.0.CO;2.

Pellicciotti F, Brock BW, Strasser U, Burlando P, Funk M, Corripio J. 2005. An enhanced temperature-index glacier melt model including the shortwave radiation balance: development and testing for Haut Glacier d' Arolla, Switzerland. *Journal of Glaciology* **51**: 573–587. DOI: 10.3189/172756505781829124.

Radić V, Hock R. 2011. Regionally differentiated contribution of mountain glaciers and ice caps to future sea-level rise. *Nature Geoscience* **4**: 91–94. DOI: 10.1038/ngeo1052.

Raper SCB, Braithwaite RJ. 2006. Low sea level rise projections from mountain glaciers and icecaps under global warming. *Nature* **439**: 311–313. DOI: 10.1038/nature04448.

Sedlar J, Hock R. 2009. Testing longwave radiation parameterizations under clear and overcast skies at Storglaciären, Sweden. *The Cryosphere* **3**: 75–84. DOI: 10.5194/tc-3-75-2009.

Serreze M, Barrett A, Stroeve J, Kindig D, Holland M. 2009. The emergence of surface-based Arctic amplification. *The Cryosphere* **3**: 11–19. DOI: 10.5194/tc-3-11-2009.

Sheridan SC. 2002. The redevelopment of a weather-type classification scheme for North America. *International Journal of Climatology* **22**: 51–68. DOI: 10.1002/joc.709.

Van den Dool HM. 1994. Searching for analogues, how long must we wait? *Tellus A* **46**: 314–324. DOI: 10.1034/j.1600-0870.1994.t01-2-00006.x.

Wilby RL. 1997. Nonstationarity in daily precipitation series: implications for GCM downscaling using atmospheric circulation indices. *International Journal of Climatology* **17**: 439–454. DOI: 10.1002/(SICI)1097-0088(19970330)17:4<439::AID-JOC145>3.0.CO;2-U.

Willis IC, Arnold NS, Brock BW. 2002. Effect of snowpack removal on energy balance, melt and runoff in a small supraglacial catchment. *Hydrological Processes* **16**: 2721–2749. DOI: 10.1002/hyp.1067.

Willmott CJ, Ackleson SG, Davis RE, Feddema JJ, Klink KM, Legates DR, Rowe CM. 1985. Statistics for the evaluation and comparison of models. *Journal of Geophysical Research: Oceans (1978–2012)* **90**: 8995–9005. DOI: 10.1029/JC090iC05p08995.

Young KC. 1994. A multivariate chain model for simulating climatic parameters from daily data. *Journal of Applied Meteorology* **33**: 661–671. DOI: 10.1175/15200450(1994)033<0661:AMCMFS>2.0.CO;2.

Zhang S, Ye B, Liu S, Zhang X, Hagemann S. 2012. A modified monthly degree-day model for evaluating glacier runoff changes in China. Part I: model development. *Hydrological Processes* **26**: 1686–1696. DOI: 10.1002/hyp.82.